energies

MDPI

Article

Hydrogen Desorption in $Mg(BH_4)_2$-$Ca(BH_4)_2$ System

Erika M. Dematteis [1,2] and Marcello Baricco [1,*]

[1] Department of Chemistry and Inter-departmental Center Nanostructured Interfaces and Surfaces (NIS), University of Turin, Via Pietro Giuria 7, 10125 Torino, Italy
[2] Université Paris Est, Institut de Chimie et des Matériaux Paris Est, ICMPE, CNRS-UPEC, F-94320 Thiais, France
* Correspondence: marcello.baricco@unito.it; Tel.: +39-011-6707569

Received: 23 July 2019; Accepted: 20 August 2019; Published: 22 August 2019

Abstract: Magnesium borohydride, $Mg(BH_4)_2$, and calcium borohydride, $Ca(BH_4)_2$, are promising materials for hydrogen storage. Mixtures of different borohydrides have been the subject of numerous researches; however, the whole $Mg(BH_4)_2$-$Ca(BH_4)_2$ system has not been investigated yet. In this study, the phase stability and the hydrogen desorption were experimentally investigated in the $Mg(BH_4)_2$-$Ca(BH_4)_2$ system, by means of XRD, ATR-IR, and HP-DSC. $Mg(BH_4)_2$ and $Ca(BH_4)_2$ are fully immiscible in the solid state. In the mechanical mixtures, thermal decomposition occurs at slightly lower temperatures than for pure compounds. However, they originate products that cannot be identified by XRD, apart from Mg and MgH_2. In fact, amorphous phases or mixtures of different poorly crystalline or nanocrystalline phases are formed, leading to a limited reversibility of the system.

Keywords: complex hydrides; magnesium borohydride; calcium borohydride; hydrogen storage; phase diagram

1. Introduction

Magnesium borohydride, $Mg(BH_4)_2$, and calcium borohydride, $Ca(BH_4)_2$, have a gravimetric hydrogen content of 14.9 and 11.6 wt%, respectively [1]. Therefore, they are very promising materials for the storage of hydrogen. Theoretical calculations predict decomposition reactions for pure $Mg(BH_4)_2$ and $Ca(BH_4)_2$ at mild temperatures [2], but the kinetics of such reactions can be very slow, thus hindering their practical use. However, little is known about their mixtures and corresponding decomposition mechanisms. In this scenario, it becomes necessary to have an in-depth understanding of the decomposition reactions mechanisms of $Mg(BH_4)_2$ and $Ca(BH_4)_2$ mixtures upon annealing, which includes a description of phase transitions, intermediate species, and final products [1,3].

Pure $Mg(BH_4)_2$ and $Ca(BH_4)_2$ starts to decompose at about 300 °C [4]. Hydrogen release reactions are rather complex and are characterized by different steps, which occur at higher temperatures and are reversible only at high pressures. Decomposition reactions may also involve the formation of diborane gas (B_2H_6) which, due to its toxicity, hinders the practical use of such materials [3,5]. It has been shown experimentally that hydrogen desorption can occur according to multiple mechanisms and in several steps, which can involve simultaneous reactions and different intermediates [6]. Several reaction paths have been proposed in the literature to explain the thermal decomposition of $Mg(BH_4)_2$ and $Ca(BH_4)_2$, including the following reactions [7–9]:

$$Mg(BH_4)_2 \rightarrow MgB_2 + 4H_2 \quad (1)$$

$$Mg(BH_4)_2 \rightarrow Mg + 2B + 4H_2 \quad (2)$$

$$Mg(BH_4)_2 \rightarrow MgH_2 + 2B + 3H_2 \quad (3)$$

$$Ca(BH_4)_2 \rightarrow \frac{1}{3}CaB_6 + \frac{2}{3}CaH_2 + \frac{10}{3}H_2 \quad (4)$$

$$Ca(BH_4)_2 \rightarrow CaH_2 + 2B + 3H_2 \quad (5)$$

$$Ca(BH_4)_2 \rightarrow Ca + 2B + 4H_2 \quad (6)$$

Mechanisms and decomposition products depend on experimental conditions and several intermediates have been observed, including $B_3H_8^-$, $B_{10}H_{10}^{2-}$, and $B_{12}H_{12}^{2-}$ anions [9–16], which probably hinder the reversibility of reactions. The role of different additives on the decomposition reactions of $Mg(BH_4)_2$ and $Ca(BH_4)_2$ has been also widely investigated [17,18].

Mixtures of borohydrides may have an easier release of hydrogen than that of the individual constituents. In fact, the formation of solid solutions can lead to a lowering of the decomposition temperatures and a change of reaction mechanisms [19–21]. According to the Density Functional Theory (DFT) calculations of Ozolins et al. [2], mixtures of $Mg(BH_4)_2$ and $Ca(BH_4)_2$ have better thermodynamic properties with respect to pure components. For the 5:1 $Mg(BH_4)_2$: $Ca(BH_4)_2$ mixture, the release of 7.73 wt% of hydrogen is expected at −18 °C and 1 bar, with an enthalpy of about 25 kJ/mol H_2, according to the following reaction:

$$5Mg(BH_4)_2 + Ca(BH_4)_2 \rightarrow CaB_{12}H_{12} + 5MgH_2 + 13H_2 \quad (7)$$

In fact, experiments of Ibikunle et al. [20,22] showed that the 5:1 $Mg(BH_4)_2$: $Ca(BH_4)_2$ mixture, after ball milling, releases hydrogen at a lower temperature and with a faster kinetic compared to the pure borohydrides. These studies showed that the 5:1 mixture begins to decompose at a temperature of 150 °C, but the system is only partially reversible, probably due to the formation of intermediates containing the $B_{12}H_{12}^{2-}$ anion, that causes a kinetic barrier for re-hydrogenation. The presence of Ca^{2+} in the mixture seems to have a beneficial effect on the mobility of the species that diffuse in $Mg(BH_4)_2$, leading to an improvement of kinetics of hydrogen desorption reactions.

Mixtures of different borohydrides have been the subject of numerous researches [1,4,23], however the whole $Mg(BH_4)_2$-$Ca(BH_4)_2$ system has not been investigated yet. In particular, no information is reported in the literature on the corresponding phase diagram. In fact, while several binary systems among alkali and/or alkali-metal borohydrides have already been characterized [24–28], a systematic study on $Mg(BH_4)_2$-$Ca(BH_4)_2$ mixtures has not been reported for all temperatures and for the full composition range. For this reason, in this paper, the phase stability and the hydrogen desorption was experimentally investigated in the $Mg(BH_4)_2$-$Ca(BH_4)_2$ system, which appears particularly promising for hydrogen storage. Pure compounds and three different mixtures were considered. Even though the reversibility of the hydrogen sorption reactions for $Mg(BH_4)_2$ and $Ca(BH_4)_2$ at high temperatures and pressures has been demonstrated [17,18], no evidences have been provided at mild conditions, which are of interest for practical applications in hydrogen storage. For this reason, the reversibility of hydrogen sorption reactions were investigated at 2 bar of H_2. Samples were investigated by means of DSC, to study the thermal behaviour of hydrogen sorption reactions, XRD, to determine the formation of crystalline phases, and ATR-IR, for the analysis of possible interactions in the mixtures.

2. Materials and Methods

Magnesium borohydride (α-$Mg(BH_4)_2$, purity >99% from KatChem) and calcium borohydride (mixed α- and β-$Ca(BH_4)_2$, purity >99% from KatChem) were fine ground by ball milling to obtain homogenous mixtures. Three $Mg(BH_4)_2$: $Ca(BH_4)_2$ mixtures (1:2, 1:1, and 2:1) have been investigated. A Fritsch Pulverisette 6 planetary was used to mill the mixtures under an inert atmosphere of nitrogen in 80 mL tungsten carbide (WC) containers and with WC balls (o.d. 10 mm). A balls-to-sample mass ratio of 46:1 was used and around 0.5 g of powders were continuously milled for 30 min, using a speed of 500 rpm. For comparison, pure compounds alone were milled in the same conditions. Because of the high reactivity to moisture of borohydrides, all preparations and manipulations of samples were

performed in nitrogen-filled glove boxes with a circulation purifier, with O_2 and H_2O levels lower than 1 ppm.

Powder X-ray diffraction (PXD) measurements were performed at room temperature using a Panalytical X-pert (Cu K_α = 1.54059 Å, K_β = 1.54446 Å) in a capillary transmission set-up (Debye-Scherer geometry). Patterns were collected from 10° to 80° 2θ range, using a step size of 0.016° and a time step of 60 s. Samples were mounted in the glove box in 0.5 mm glass capillaries and sealed with plastiline, then moved out of the glove box and sealed with flame. All PXD data have been refined by the Rietveld method using the MAUD program [29].

A high-pressure 204 Netsch DSC (HP-DSC), located inside a nitrogen-filled glovebox, was used to analyse all samples. To clarify the reversibility of phase transformations, three cycles of heating and cooling from room temperature up to 210 °C at 5 °C/min with a hydrogen pressure of 2 bar were performed. In order to investigate thermal decomposition reactions, thermal cycling up to 420 °C at 5 °C/min, under 2 bar of H_2, was also carried out.

Infrared spectra (2 cm^{-1} resolution, average on 64 scans) were collected in Attenuated Total Reflection mode on loose powder, using a Bruker Alpha-P spectrometer, equipped with a diamond crystal. All spectra were recorded in the 5000–400 cm^{-1} range in a protected atmosphere, since the instrument was placed inside a nitrogen filled glove-box (MBraun Lab Star Glove Box supplied with pure 5.5 grade Nitrogen, <1 ppm O_2, <1 ppm H_2O).

3. Results and Discussion

3.1. Synthesis, Structural and Thermal Characterization

From the PXD diffraction patterns shown in Figure 1, it is possible to notice that only the α phase is present after ball-milling pure $Mg(BH_4)_2$, while both α and β polymorphs are clearly visible after ball-milling pure $Ca(BH_4)_2$. Only diffraction peaks of these three phases are present in PXD patterns of mixtures, as shown in Figure 1, suggesting that $Mg(BH_4)_2$ and $Ca(BH_4)_2$ are immiscible in the whole composition range, even after a ball-milling treatment.

ATR-IR spectra of pure compounds and mixtures after ball-milling are reported in Figure 2. Bands in the 2500–2000 cm^{-1} range are related to the stretching of the B-H bond of the BH_4^- anion, while those present between 1500–1000 cm^{-1} are due to the H-B-H bending of the same anion [4,30,31]. For pure $Ca(BH_4)_2$, a splitting of stretching bands is evident. This is due to the presence of both polymorphs α and β [31]. The band at 2319 cm^{-1} (marked as (i) in Figure 2) is associated to α-$Ca(BH_4)_2$, while that at 2253 cm^{-1} (marked as (ii) in Figure 2) is related to β-$Ca(BH_4)_2$ [32]. Bending band for pure $Ca(BH_4)_2$ is composed by a main component at 1194 cm^{-1} (marked as (iii) in Figure 2), coupled by various satellite bands (marked as (iv), 1109 cm^{-1}, and (v), 1074 cm^{-1}, in Figure 2) [30–33]. ATR-IR spectrum of pure $Mg(BH_4)_2$ shows a single stretching band at 2272 cm^{-1} (marked as (vi) in Figure 2), confirming the presence of the single α phase [31,34–36]. Similarly, a main bending band is observed for pure $Mg(BH_4)_2$ at 1256 cm^{-1} (marked as (vii) in Figure 2).

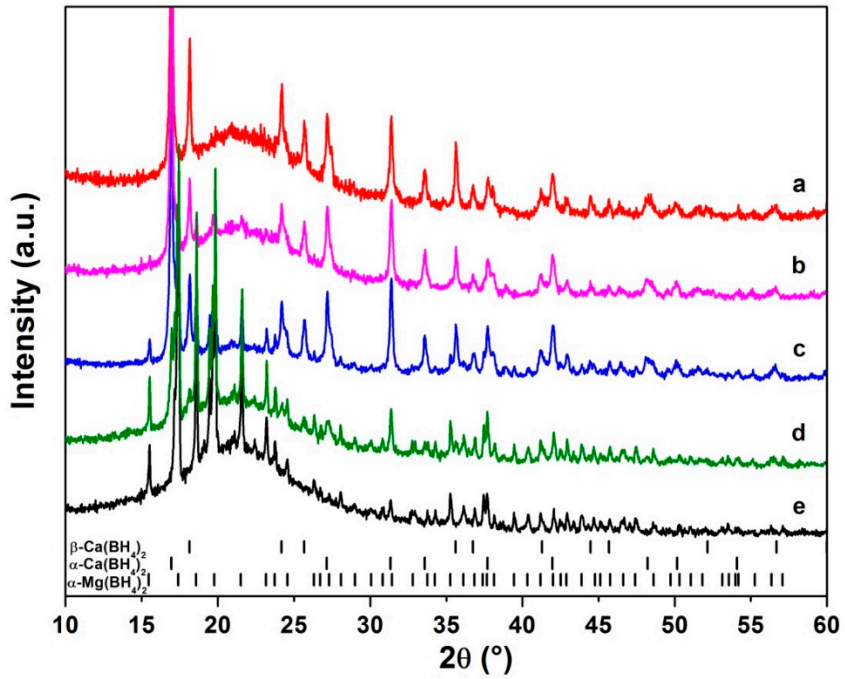

Figure 1. Powder X-ray diffraction (PXD) patterns of (a) $Ca(BH_4)_2$, (b) $1Mg(BH_4)_2$: $2Ca(BH_4)_2$, (c) $1Mg(BH_4)_2$: $1Ca(BH_4)_2$, (d) $2Mg(BH_4)_2$: $1Ca(BH_4)_2$, and (e) $Mg(BH_4)_2$ after ball milling.

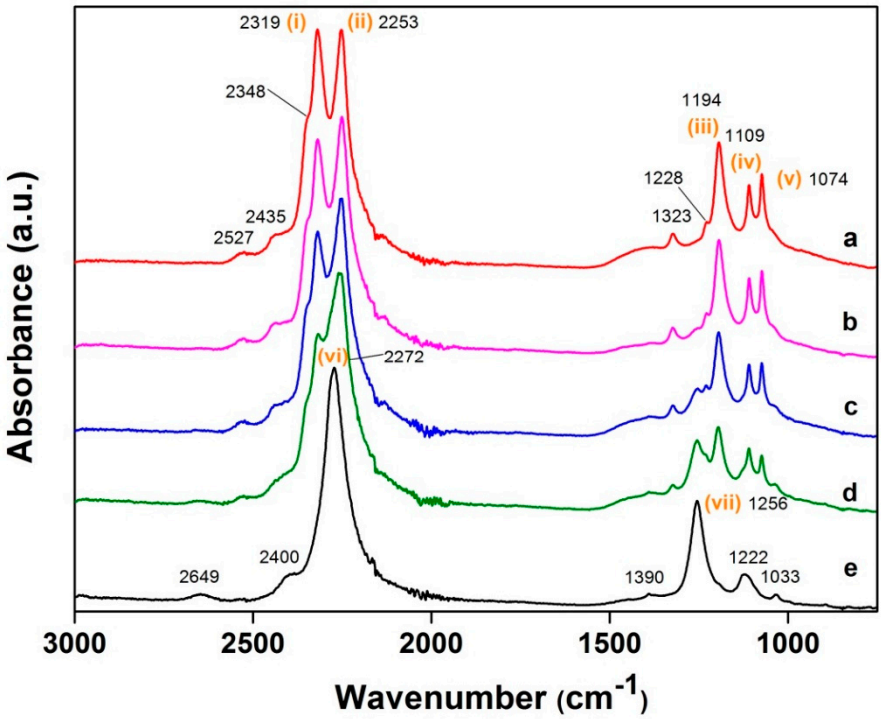

Figure 2. ATR-IR spectra of (a) $Ca(BH_4)_2$, (b) $1Mg(BH_4)_2$: $2Ca(BH_4)_2$, (c) $1Mg(BH_4)_2$: $1Ca(BH_4)_2$, (d) $2Mg(BH_4)_2$: $1Ca(BH_4)_2$ and (e) $Mg(BH_4)_2$ after ball milling. For bands labelling, see the text.

ATR-IR spectra of 2:1, 1:1, 1:2 mixtures appear to be very similar to those of pure compounds, confirming that all mixtures contain α-$Mg(BH_4)_2$ and both α-$Ca(BH_4)_2$ and β-$Ca(BH_4)_2$ phases, as already evidenced from PXD patterns (Figure 1). However, for the mixture 2:1, the separation between the two bands is less evident in the 2350–2250 cm^{-1} region (Figure 2) with respect to pure $Ca(BH_4)_2$, while they are better separated in the 1:1 and 1:2 mixtures. In fact, increasing the $Mg(BH_4)_2$

content in the mixture, the band (b) is slightly shifted to larger wave numbers with respect to pure $Ca(BH_4)_2$, thus overlapping to band (f), at 2272 cm^{-1}. In addition, band (g) becomes clearly observable at about 1254 cm^{-1}. Therefore, it can be concluded that the spectroscopic analysis confirms the immiscibility of α-$Mg(BH_4)_2$ with both α-$Ca(BH_4)_2$ and β-$Ca(BH_4)_2$, since the observed signals are basically a combination of those of single phases.

The DSC traces observed during the first heating ramp are reported in Figure 3 and corresponding PXD patterns, obtained after three cycles of heating and cooling from room temperature up to 210 °C at 5 °C/min with a hydrogen pressure of 2 bar, are reported in Figure 4.

The $Mg(BH_4)_2$ α-β transition temperature is clearly recorded at T_{peak} = 191 °C (T_{onset} = 181 °C), as it can be observed in Figure 3. On the other hand, in the DSC trace of $Ca(BH_4)_2$, only a broad peak around 168 °C (T_{onset} = 157 °C) can be observed, corresponding to the α-β transformation. The α-β phase transition in pure $Mg(BH_4)_2$ and $Ca(BH_4)_2$ is not fully reversible, because no signals were recorded in DSC traces during cooling (not shown). In fact, in the PXD patterns of ball-milled $Mg(BH_4)_2$ after heat treatment (Figure 4), only peaks of the β phase, metastable at room temperature, are distinguished. For $Ca(BH_4)_2$, after the DSC cycling, both α and β phases are present, as shown in Figure 4, where the PXD pattern is similar to that observed after the ball-milling treatment (Figure 1). It should be noted, however, that the ratio between the intensities of the PXD peaks around 17° and 18°, $\left(I_{\beta\ Ca}/I_{\alpha\ Ca}\right)$, corresponding to the β-$Ca(BH_4)_2$ and the α-$Ca(BH_4)_2$ phases, respectively, increases considerably, as it is clearly observed comparing the PXD patterns in Figures 1 and 4. This result suggests that thermal cycling is more effective than ball-milling in stabilizing at room temperature the β phase in $Ca(BH_4)_2$.

Two endothermic peaks are always observed in the DSC traces of the mixtures (Figure 3). At lower temperatures, the broad peak refers to the α-β transition of $Ca(BH_4)_2$, while the second more intense and narrow peak is linked to the α-β polymorphic transition of $Mg(BH_4)_2$, as described before. In the PXD patterns after DSC cycling (Figure 4), β-$Mg(BH_4)_2$, α-$Ca(BH_4)_2$, and β-$Ca(BH_4)_2$ are observed, with an increase of the $\left(I_{\beta\ Ca}/I_{\alpha\ Ca}\right)$ intensity ratio with respect to as milled samples (Figure 1), as already observed for pure $Ca(BH_4)_2$. The presence of both $Mg(BH_4)_2$ and $Ca(BH_4)_2$ in the mixture could influence the mechanism of the individual phase transitions. When $Mg(BH_4)_2$ is present, the α-β transition of $Ca(BH_4)_2$ occurs at a slightly lower temperatures (Table 1) and in a narrower temperature interval with respect to the pure compound, as can be observed in Figure 3. The α-β transformation of $Mg(BH_4)_2$, on the other hand, does not evidence any particular changes. In fact, the DSC peak temperature is slightly increased with respect to the pure compound only for the 1:2 mixture (Figure 3 and Table 1). In conclusion, the signals of the mixtures do not change significantly, confirming that no solid solutions can be formed upon ball milling.

The cell parameters and volumes per formula unit of α-, β-$Mg(BH_4)_2$ (Table 2) and α-, β-$Ca(BH_4)_2$ (Table 3) were obtained by the Rietveld refinement of PXD patterns for all samples after ball milling and DSC cycling. Cell volumes per formula unit remain unchanged, underlining the immiscibility of $Mg(BH_4)_2$ and $Ca(BH_4)_2$ even after thermal treatment up to 210 °C.

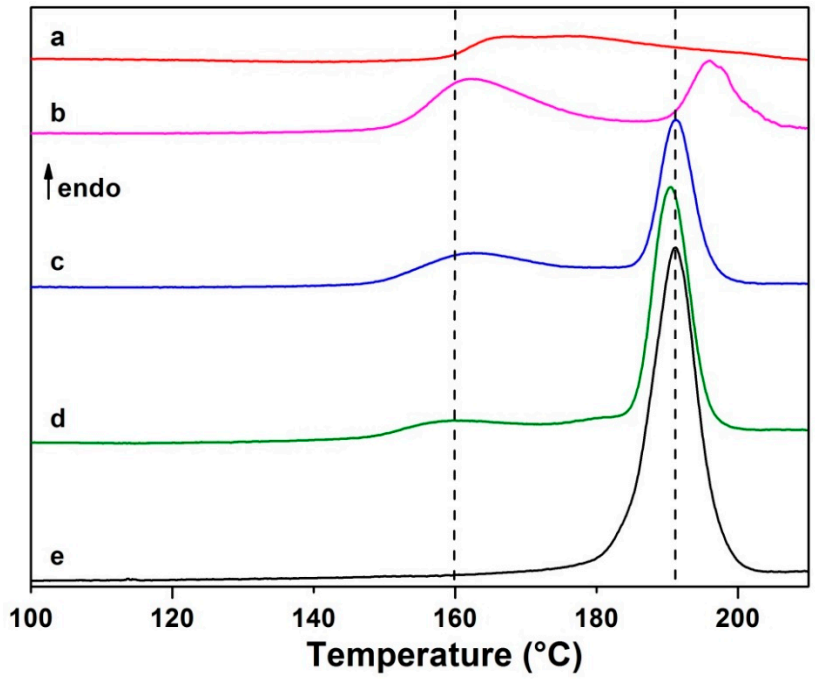

Figure 3. DSC analysis up to 210 °C at 5 °C/min, under 2 bar of H_2, of (a) $Ca(BH_4)_2$, (b) $1Mg(BH_4)_2$: $2Ca(BH_4)_2$, (c) $1Mg(BH_4)_2$: $1Ca(BH_4)_2$, (d) $2Mg(BH_4)_2$: $1Ca(BH_4)_2$, and (e) $Mg(BH_4)_2$ after ball milling. Only the first heating ramp is reported.

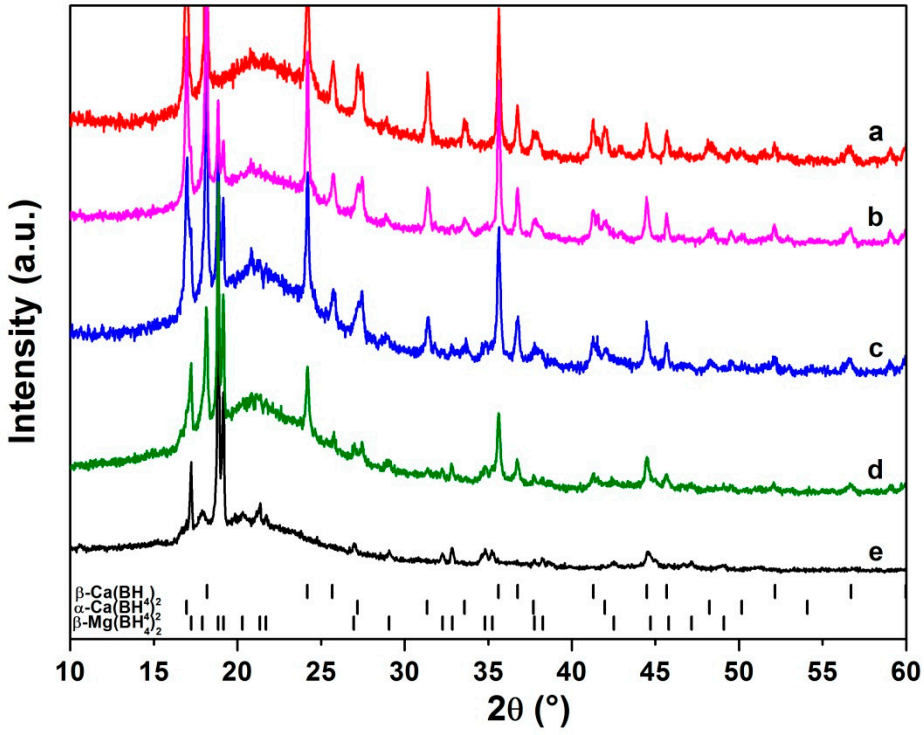

Figure 4. Room temperature PXD pattern of (a) $Ca(BH_4)_2$, (b) $1Mg(BH_4)_2$: $2Ca(BH_4)_2$, (c) $1Mg(BH_4)_2$: $1Ca(BH_4)_2$, (d) $2Mg(BH_4)_2$: $1Ca(BH_4)_2$ and (e) $Mg(BH_4)_2$ after DSC cycling up to 210 °C under 2 bar of H_2.

Table 1. Onset and peak temperatures of α-β polymorphic transition, decomposition, and re-hydrogenation of pure $Mg(BH_4)_2$, $Ca(BH_4)_2$ and their mixtures (2:1, 1:1, 1:2 molar ratio), obtained in the DSC analysis under 2 bar of H_2 reported in Figures 3 and 5. PT = phase transition; Dec. = thermal decomposition; Re-H_2 = rehydrogenation.

Sample	T_{onset} (°C) $Ca(BH_4)_2$ α-β PT	T_{peak} (°C) $Ca(BH_4)_2$ α-β PT	T_{onset} (°C) $Mg(BH_4)_2$ α-β PT	T_{peak} (°C) $Mg(BH_4)_2$ α-β PT	T_{peak} (°C) Dec.	T_{onset} (°C); T_{peak} (°C) Re-H_2
$Mg(BH_4)_2$			181	191	299, 340, 355, 386	278; 254
2:1	149	160		191	272, 326, 346, 398	288; 273
1:1	149	163		191	282, 390	
1:2	149	162		196	280, 387	
$Ca(BH_4)_2$	157	168			355, 376	

Table 2. Cell parameters (*a*,*c*) and volumes per formula unit (*V*/*z*) obtained from Rietveld refinement of α (z = 30) and β (z = 64) phases of $Mg(BH_4)_2$ after BM and DSC cycling under 2 bar of H_2 for pure $Mg(BH_4)_2$ and mixtures (2:1, 1:1, 1:2 molar ratio $Mg(BH_4)_2$:$Ca(BH_4)_2$). After BM, only the α phase was present, while after DSC cycling under 2 bar of H_2 only the β phase was observed.

Sample		α-$Mg(BH_4)_2$			β-$Mg(BH_4)_2$			
		a (Å)	*c* (Å)	*V*/*z* (Å^3)	*a* (Å)	*b* (Å)	*c* (Å)	*V*/*z* (Å^3)
$Mg(BH_4)_2$	BM	10.347	37.115	475				
	DSC				37.098	18.626	10.917	118
2:1	BM	10.344	37.102	475				
	DSC				37.105	18.640	10.921	118
1:1	BM	10.345	37.103	475				
	DSC				37.107	18.647	10.921	118
1:2	BM	10.342	37.088	474				
	DSC				37.089	18.667	10.921	118

Table 3. Cell parameters (*a*,*b*,*c*) and volumes per formula unit (*V*/*z*) obtained from Rietveld refinement of PXD patterns for α (z = 30) and β (z = 64) $Ca(BH_4)_2$ after BM and DSC cycling under 2 bar of H_2 for pure $Ca(BH_4)_2$ and mixtures (2:1, 1:1, 1:2 molar ratio $Mg(BH_4)_2$:$Ca(BH_4)_2$). After BM and DSC cycling under 2 bar of H_2, both α the β phases were observed.

Sample		α-$Ca(BH_4)_2$				β-$Ca(BH_4)_2$		
		a (Å)	*b* (Å)	*c* (Å)	*V*/*z* (Å^3)	*a* (Å)	*c* (Å)	*V*/*z* (Å^3)
2:1	BM	8.776	13.127	7.497	108	6.911	4.350	65
	DSC	8.744	13.104	7.480	107	6.918	4.348	65
1:1	BM	8.777	13.125	7.496	108	6.914	4.346	65
	DSC	8.754	13.105	7.497	108	6.917	4.348	65
1:2	BM	8.775	13.125	7.499	108	6.915	4.347	65
	DSC	8.760	13.116	7.503	108	6.917	4.347	65
$Ca(BH_4)_2$	BM	8.775	13.125	7.499	108	6.915	4.346	65
	DSC	8.762	13.119	7.496	108	6.917	4.348	65

Ionic compounds with similar crystalline structures, electronegativity, and cation size imply minimum distortions and maximum packaging, promoting the formation of solid solutions [4]. The hindered formation of solid solutions in the $Mg(BH_4)_2$-$Ca(BH_4)_2$ system can be explained on the basis of differences in crystal structure of α,β-$Mg(BH_4)_2$ [37] and α,β-$Ca(BH_4)_2$ [38], in the coordination number (CN) of cations (CN=4 for $Mg(BH_4)_2$ and CN=6 for $Ca(BH_4)_2$) and in ionic radius

(rMg^{2+} = 57 pm and rCa^{2+} = 100 pm) [39]. It is worth noting that Mg^{2+} and Ca^{2+} ions are iso-valent, whereby the immiscibility of $Mg(BH_4)_2$ and $Ca(BH_4)_2$ cannot be explained by electronic factors [4].

3.2. Thermal Decomposition

DSC traces observed during a heating and cooling cycle from room temperature up to 420 °C at 5 °C/min, under 2 bar of H_2, are reported in Figure 5 and corresponding PXD patterns, obtained after the thermal treatment, are reported in Figure 6.

The thermal decomposition of pure $Mg(BH_4)_2$ occurs in four steps. In fact, during heating, endothermic signals at peak temperatures of 299 (T_{onset} = 269 °C), 340, 355, and 386 °C can be observed in Figure 5, in addition to the peak at 193 °C, corresponding to the α-β phase transition already described before. Upon cooling, a single exothermic peak due to re-hydrogenation is observed at 254 °C (T_{onset} = 278 °C). The phases identified after the thermal decomposition and rehydrogenation of $Mg(BH_4)_2$ are Mg and MgH_2 (Figure 6).

Observed experimental data confirm investigations previously reported in the literature [3,5,13,40]. $Mg(BH_4)_2$ has a complex decomposition mechanism, in which several intermediates are involved, creating an obstacle to the complete reversibility of the hydrogen sorption reactions. Intermediate compounds have not been clarified yet and they depend on experimental conditions [6]. In some studies, the formation of $Mg(B_3H_8)_2$ was observed [41,42]. However, its formation does not seem to be spontaneous [8], even if from DFT calculations it appears very stable [10]. Other suggested intermediate phases are $MgB_{10}H_{10}$ [11,16], MgB_4H_{10} [11], $MgB_{12}H_{12}$ [13], and a generic MgB_xH_y phase [12].

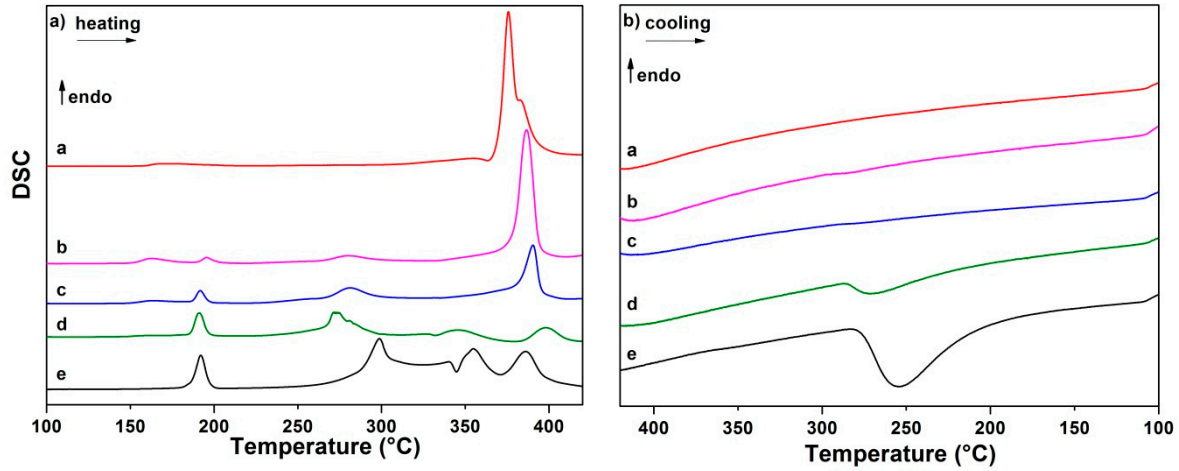

Figure 5. DSC analysis up to 420 °C at 5 °C/min, under 2 bar of H_2, of (a) $Ca(BH_4)_2$, (b) $1Mg(BH_4)_2$: $2Ca(BH_4)_2$, (c) $1Mg(BH_4)_2$: $1Ca(BH_4)_2$, (d) $2Mg(BH_4)_2$: $1Ca(BH_4)_2$, and (e) $Mg(BH_4)_2$. (**a**) heating and (**b**) cooling ramp.

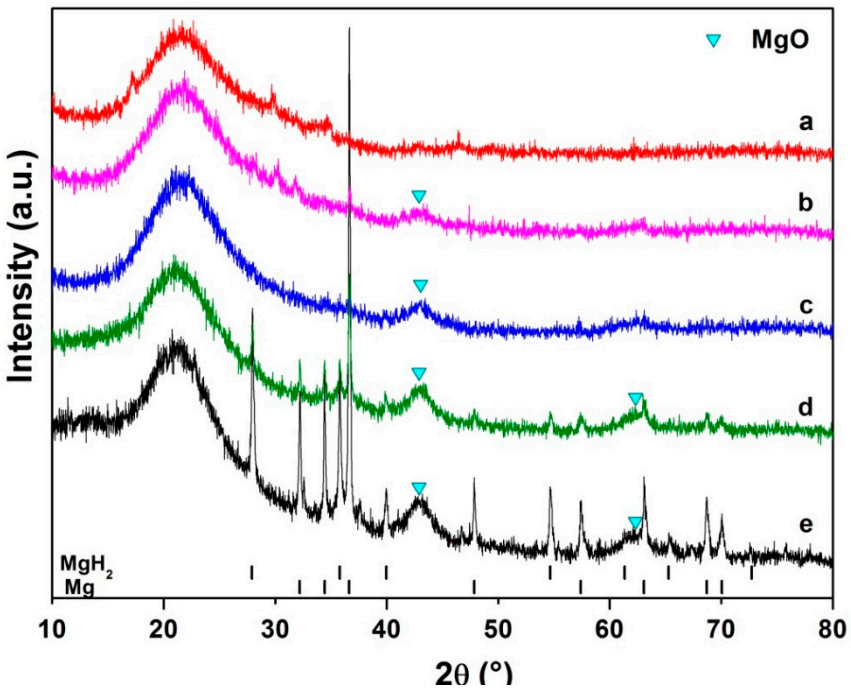

Figure 6. Room temperature PXD pattern of (a) $Ca(BH_4)_2$, (b) $1Mg(BH_4)_2$: $2Ca(BH_4)_2$, (c) $1Mg(BH_4)_2$: $1Ca(BH_4)_2$, (d) $2Mg(BH_4)_2$: $1Ca(BH_4)_2$, and (e) $Mg(BH_4)_2$ after thermal cycling (DSC analysis up to 440 °C under 2 bar of H_2).

From the collected data, it is possible to confirm a four-step process [13], which starts at 270 °C. In the first two steps, intermediate products are formed, which could be linked to amorphous phases [11–13]. At 355 °C, MgH_2 is formed, which then decomposes into Mg. The exothermic peak observed in the DSC trace on cooling in Figure 5, is related to its rehydrogenation reaction into MgH_2 [13]. Because of the low hydrogen pressure applied (2 bar), it was not possible to fully hydrogenate all the magnesium produced during the thermal decomposition. In fact, both Mg and MgH_2 phases are observed in the PXD pattern after the thermal cycle (Figure 6). The formation of Mg and MgH_2 from the thermal decomposition and re-hydrogenation of $Mg(BH_4)_2$ has been observed in several studies [11–13,43]. It seems that MgH_2 does not appear as a product of the first reaction steps, but it is formed at temperatures higher than 280 °C [12]. In conclusion, it is confirmed that the decomposition of pure $Mg(BH_4)_2$ cannot be simply explained through the following reactions

$$Mg(BH_4)_2 \rightarrow MgH_2 + 2B + 3H_2 \rightarrow Mg + 2B + 4H_2 \quad (8)$$

and that the formation of particularly stable intermediates could be the reason of the incomplete reversibility of the reactions [2,7,11,12,44].

The decomposition of pure $Ca(BH_4)_2$ proceeds through two steps, as observed by Mao et al. [45] and Riktor et al. [43]. In the DSC trace, in addition to the α-β transition at 168 °C (barely visible in Figure 5), two endothermic DSC signals at 355 °C (low intensity) and at 376 °C (main peak) can be evidenced. In this case, it is difficult to determine the decomposition products, because no diffraction peaks are clearly visible in the PXD patterns after decomposition (Figure 6). Thus, amorphous products could be involved, such as $CaB_{12}H_{12}$ or other compounds containing Ca, B, and H, which, however, do not have long-range order [7,9,14].

In the literature, different decomposition steps have been suggested for $Ca(BH_4)_2$ [2] according to the following reactions:

$$6Ca(BH_4)_2 \rightarrow CaB_{12}H_{12} + 5CaH_2 + 13H_2 \rightarrow CaB_6 + 2CaH_2 + 10H_2 \quad (9)$$

No diffraction peaks associated to the CaB_6 can be observed in the PXD analysis after thermal cycling (Figure 6). This observation supports the results of Kim et al. [46], where it has been shown that $Ca(BH_4)_2$ decomposes into nanocrystalline CaB_6, which cannot be easily identified by PXD. Additionally, the decomposition could follow a different path, forming phases containing Ca, B, and H, such as amorphous $CaB_{12}H_{12}$ [47] or crystalline $CaB_{12}H_{12}$, CaB_6 and CaH_2 [15].

In the 2:1 mixture, the thermal decomposition follows four steps (Figure 5). DSC trace upon heating is similar to that of pure $Mg(BH_4)_2$, even if peak temperatures result at slightly lower values for the mixture with respect to the pure compound, while the last peak is shifted to higher temperatures (Table 1). The decomposition is partially reversible, as can be seen from the exothermic peak upon cooling (Figure 5) at 273 °C (T_{onset} = 288 °C), corresponding to the re-hydrogenation of magnesium, similarly to pure $Mg(BH_4)_2$ [13]. In fact, MgH_2 and Mg can be identified from the diffraction pattern after thermal cycling (Figure 6). Also in this case, it is not possible to exclude the formation of amorphous phases, which may prevent the full reversibility of hydrogen sorption reaction of $Mg(BH_4)_2$ [2,7,11,12,44]. Nevertheless, the presence of $Ca(BH_4)_2$ in the mixture, promotes the decomposition of $Mg(BH_4)_2$ at lower temperature and involves a wider temperature range with respect to the pure compound, as it can be seen from Figure 5. Ibikunle et al. [20], studying the 5:1 $Mg(BH_4)_2$:$Ca(BH_4)_2$ mixture, also underlined that the presence of two borohydrides result in a hydrogen release at lower temperature with respect to pure compounds. Since no crystalline phases containing calcium have been found, the fraction of $Ca(BH_4)_2$ present in the mixture likely decomposed independently, thus being responsible for peaks broadening in the DSC trace.

In 1:1 and 1:2 mixtures, the decomposition mechanism is characterized by two steps, with DSC peak temperatures T_{peak} equal to 280 °C and 390 °C, with the second peak more intense than the first one. The identification of decomposition products is rather difficult from PXD patterns (Figure 6), since no crystalline peaks can be observed. In fact, similarly to pure $Ca(BH_4)_2$, the formation of amorphous or nano-crystalline phases could take place during thermal decomposition. Because of the strong similarity of DSC signals (Figure 5) and diffraction patterns (Figure 6) in these two mixtures, it is reasonable to consider similar mechanisms and reaction products. As $Ca(BH_4)_2$ decomposes after $Mg(BH_4)_2$, it is feasible that the products formed in the first decomposition step of $Mg(BH_4)_2$ could react with $Ca(BH_4)_2$ to form new phases, which are stable up to 390 °C. If MgH_2 formation is considered for the first decomposition step of $Mg(BH_4)_2$, the reaction mechanism could be traced back to that of $Ca(BH_4)_2$-MgH_2 mixtures [15,46,48]. According to Kim et al. [46] and Minella et al. [15,48], the formation of Mg-Ca-H phases is firstly observed, followed by the occurrence of $CaB_{12}H_{12}$, amorphous CaB_6 and CaH_2, as well as crystalline Mg. The decomposition of the 1:1 and 1:2 mixtures is not reversible in the present experimental conditions, as confirmed by the absence of peaks in the DSC traces upon cooling (Figure 5).

Comparing the patterns of various mixtures in Figure 6, broad diffraction peaks at about 43° and 62° are present, whose intensities decrease with the decreasing content of $Mg(BH_4)_2$ in the mixture. They correspond to traces of MgO, due to the oxidation of magnesium. The formation of MgO may be likely due to contamination of the starting ball milled sample. Its formation during heating is in fact extremely favoured and could have influenced the hydrogen desorption mechanism, limiting or preventing its reversibility [11].

ATR spectra after thermal cycling in DSC up to 440 °C under 2 bar of H_2 are shown in Figure 7 and they provide some further information on thermal decomposition products. In fact, in all of them there is a broad band (I), in the 2590–2000 cm^{-1} region. This can be referred to the B–H stretching [4,14] and therefore indicates the presence of species still containing the B–H bond. Therefore, the hydrogen desorption reactions may have not been completed or some new species have been formed during re-hydrogenation. In any case, not only hydrides and borides are present as products of the thermal cycling under 2 bar of H_2. The broadening of the ATR band (I) seems to confirm the presence of multiple different phases [4]. Since the most intense ATR band of $B_{12}H_{12}^{2-}$ is located at 2480 cm^{-1}

and the calculated spectra of $B_3H_8^-$, $B_{10}H_{10}^{2-}$, and $B_4H_{10}^{2-}$ presents bands in the 2500–2000 cm^{-1} range [11,49], it is indeed possible that species containing these anions are formed.

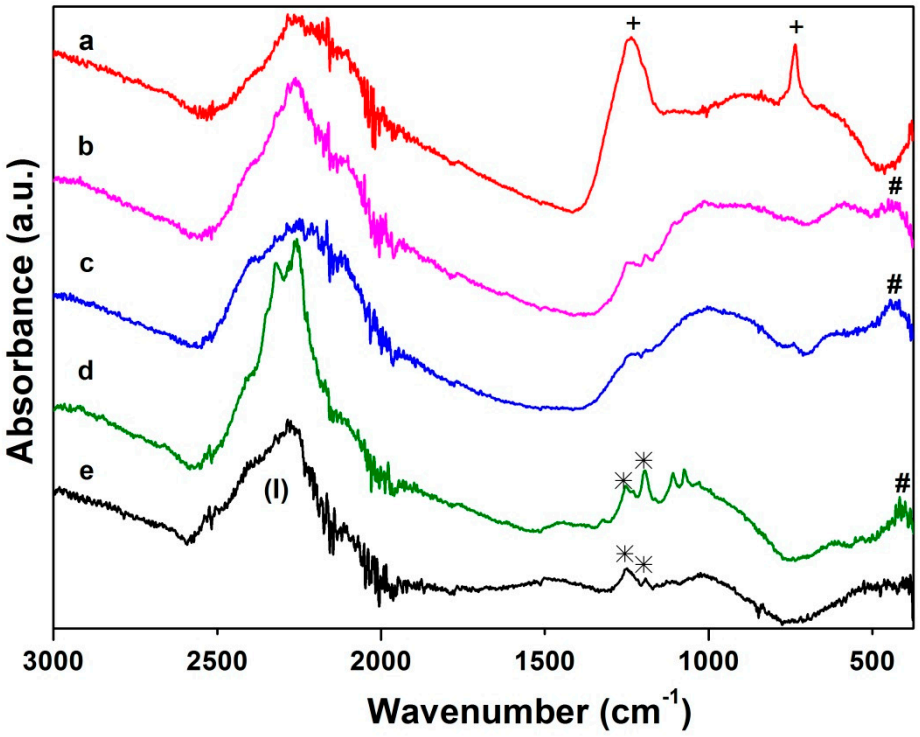

Figure 7. ATR-IR spectra of (a) $Ca(BH_4)_2$, (b) $1Mg(BH_4)_2$: $2Ca(BH_4)_2$, (c) $1Mg(BH_4)_2$: $1Ca(BH_4)_2$, (d) $2Mg(BH_4)_2$: $1Ca(BH_4)_2$, and (e) $Mg(BH_4)_2$ after thermal cycling (DSC analysis up to 440 °C under 2 bar of H_2). For symbols explanations, see the text.

In the ATR spectrum of pure $Mg(BH_4)_2$ after thermal cycling, shown in Figure 7, in addition to the band (I), two small bands at 1250 cm^{-1} and 1190 cm^{-1} (marked with *) are observed. In the ATR spectrum of pure $Ca(BH_4)_2$ after thermal cycling, also two bands are observed (marked with +), the first one at 1235 cm^{-1}, which could be related to the $B_{12}H_{12}^{2-}$ anion [11], and a second one at 736 cm^{-1}, that does not correspond to any of the bands reported in the literature for closoboranes [49].

The ATR spectrum for 2:1 mixture after thermal cycling, reported in Figure 7, shows the same bands observed for $Mg(BH_4)_2$, together with two more bands at 1109 cm^{-1} and 1074 cm^{-1}, which are difficult to be assigned. ATR spectra of 1:2 and 1:1 mixtures are very similar to each other, presenting both a broadband at about 1000 cm^{-1} less intense than (I), and another band at about 430 cm^{-1} (marked with #), which can be also observed for the 2:1 mixture, which cannot be easily assigned.

In conclusion, ATR analysis evidenced that new species are involved in the decomposition and re-hydrogenation of the mixtures in the $Mg(BH_4)_2$-$Ca(BH_4)_2$ system, which certainly contain B–H bonds.

4. Conclusions

The phase stability and the thermal hydrogen desorption was experimentally investigated in the $Mg(BH_4)_2$-$Ca(BH_4)_2$ system. $Mg(BH_4)_2$ and $Ca(BH_4)_2$ are fully immiscible in the solid state. In fact, in the XRD patterns of 1:2, 1:1, and 2:1 mixtures, collected after ball-milling and heat treatment up to 210 °C under 2 bar hydrogen pressure, the signals of the constituent phases were always distinguished. The ATR spectra and cell volumes also confirmed this conclusion.

The thermal decomposition of 2:1 mixture was similar to that of pure $Mg(BH_4)_2$, also originating the same crystalline products (Mg and MgH_2). For 1:1 and 1:2 mixtures, the decomposition displayed only two steps. The first is linked to the decomposition of $Mg(BH_4)_2$ and the second one to that

of $Ca(BH_4)_2$. In the mixtures, the thermal decomposition of $Mg(BH_4)_2$ originates, at about 280 °C, new species that reacts with $Ca(BH_4)_2$, shifting its decomposition to higher temperatures with respect to pure compounds. No products can be identified by X-ray diffraction patterns, apart from Mg and MgH_2. In fact, amorphous phases or mixtures of different poorly crystalline or nanocrystalline phases are formed. However, as shown by ATR-IR analysis, not only hydrides and borides phases are obtained after cycling up to 440 °C under 2 bar of H_2, but also species containing the B–H bond. At 2 bar of H_2, only for $Mg(BH_4)_2$ and the 2:1 mixture, the hydrogen sorption reaction is partially reversible.

In conclusion, it has been pointed out that $Mg(BH_4)_2$-$Ca(BH_4)_2$ mixtures begin to decompose at slightly lower temperatures with respect to parent borohydrides. However, the reaction is irreversible at 2 bar of hydrogen pressure, thus presenting many limitations from the point of view of practical applications as hydrogen storage materials. The very limited composition dependence of observed temperatures confirms the immiscibility of the $Mg(BH_4)_2$ and $Ca(BH_4)_2$ compounds in the solid state. Further studies are needed to clearly identify the decomposition products that were formed, because some particularly stable species hinder the reversibility of the hydrogen sorption reactions.

Author Contributions: E.M.D. and M.B. devised the experiments, E.M.D. performed experiments and analysed data, E.M.D. and M.B. discussed the data, E.M.D. wrote the manuscript and M.B. revised the manuscript.

Funding: Financial support from the European Fuel Cells and Hydrogen Joint Undertaking in the framework of the BOR4STORE (Grant agreement n° 303428) is thankfully acknowledged.

Acknowledgments: The authors acknowledge Sofia Sturari (University of Turin) for supports in experiments.

Conflicts of Interest: The authors declare no conflict of interest.

References

1. Milanese, C.; Jensen, T.R.; Hauback, B.C.; Pistidda, C.; Dornheim, M.; Yang, H.; Lombardo, L.; Zuettel, A.; Filinchuk, Y.; Ngene, P.; et al. Complex hydrides for energy storage. *Int. J. Hydrog. Energy* **2019**, *44*, 7860–7874. [CrossRef]
2. Ozolins, V.; Majzoub, E.H.; Wolverton, C. First-Principles Prediction of Thermodynamically Reversible Hydrogen Storage Reactions in the Li-Mg-Ca-B-H System. *J. Am. Chem. Soc.* **2009**, *131*, 230–237. [CrossRef] [PubMed]
3. Paskevicius, M.; Jepsen, L.H.; Schouwink, P.; Černý, R.; Ravnsbæk, D.B.; Filinchuk, Y.; Dornheim, M.; Besenbacher, F.; Jensen, T.R. Metal borohydrides and derivatives—Synthesis, structure and properties. *Chem. Soc. Rev.* **2017**, *46*, 1565–1634. [CrossRef] [PubMed]
4. Dematteis, E.M.; Santoru, A.; Poletti, M.G.; Pistidda, C.; Klassen, T.; Dornheim, M.; Baricco, M. Phase stability and hydrogen desorption in a quinary equimolar mixture of light-metals borohydrides. *Int. J. Hydrog. Energy* **2018**, *43*, 16793–16803. [CrossRef]
5. Orimo, S.-I.; Nakamori, Y.; Eliseo, J.R.; Züttel, A.; Jensen, C.M. Complex Hydrides for Hydrogen Storage. *Chem. Rev.* **2007**, *107*, 4111–4132. [CrossRef] [PubMed]
6. Rönnebro, E. Development of group II borohydrides as hydrogen storage materials. *Curr. Opin. Solid State Mater. Sci.* **2011**, *15*, 44–51. [CrossRef]
7. Kulkarni, A.D.; Wang, L.-L.; Johnson, D.D.; Sholl, D.S.; Johnson, J.K. First-Principles Characterization of Amorphous Phases of $MB_{12}H_{12}$, M = Mg, Ca. *J. Phys. Chem. C* **2010**, *114*, 14601–14605. [CrossRef]
8. Pinatel, E.R.; Albanese, E.; Civalleri, B.; Baricco, M. Thermodynamic modelling of $Mg(BH_4)_2$. *J. Alloys Compd.* **2015**, *645*, S64–S68. [CrossRef]
9. Wang, L.; Graham, D.D.; Robertson, I.M.; Johnson, D.D. On the Reversibility of Hydrogen-Storage Reactions in $Ca(BH_4)_2$: Characterization via Experiment and Theory. *J. Phys. Chem. C* **2009**, *113*, 20088–20096. [CrossRef]
10. Liu, Y.; Giri, S.; Zhou, J.; Jena, P. Intermediate Phases during Decomposition of Metal Borohydrides, $M(BH_4)n$ (M = Na, Mg, Y). *J. Phys. Chem. C* **2014**, *118*, 28456–28461. [CrossRef]
11. Vitillo, J.; Bordiga, S.; Baricco, M. Spectroscopic and Structural Characterization of Thermal Decomposition of γ-$Mg(BH_4)_2$: Dynamic Vacuum versus H_2 Atmosphere. *J. Phys. Chem. C* **2015**, *119*, 25340–25351. [CrossRef]
12. Zavorotynska, O.; Deledda, S.; Hauback, B.C. Kinetics studies of the reversible partial decomposition reaction in $Mg(BH_4)_2$. *Int. J. Hydrog. Energy* **2016**, *41*, 9885–9892. [CrossRef]

13. Soloveichik, G.L.; Gao, Y.; Rijssenbeek, J.; Andrus, M.; Kniajanski, S.; Bowman, R.C., Jr; Hwang, S.; Zhao, J. Magnesium borohydride as a hydrogen storage material: Properties and dehydrogenation pathway of unsolvated $Mg(BH_4)_2$. *Int. J. Hydrog. Energy* **2009**, *34*, 916–928. [CrossRef]
14. Riktor, M.D.; Sørby, M.H.; Muller, J.; Bardají, E.G.; Fichtner, M.; Hauback, B.C. On the rehydrogenation of decomposed $Ca(BH_4)_2$. *J. Alloys Compd.* **2015**, *632*, 800–804. [CrossRef]
15. Bonatto Minella, C.; Garroni, S.; Olid, D.; Teixidor, F.; Pistidda, C.; Lindemann, I.; Gutfleisch, O.; Baró, M.D.; Bormann, R.; Klassen, T.; et al. Experimental Evidence of $Ca[B_{12}H_{12}]$ Formation During Decomposition of a $Ca(BH_4)_2$ + MgH_2 Based Reactive Hydride Composite. *J. Phys. Chem. C* **2011**, *115*, 18010–18014. [CrossRef]
16. Saldan, I.; Hino, S.; Humphries, T.D.; Zavorotynska, O.; Chong, M.; Jensen, C.M.; Deledda, S.; Hauback, B.C. Structural Changes Observed during the Reversible Hydrogenation of $Mg(BH_4)_2$ with Ni-Based Additives. *J. Phys. Chem. C* **2014**, *118*, 23376–23384. [CrossRef]
17. Rueda, M.; Sanz-Moral, L.M.; Girella, A.; Cofrancesco, P.; Milanese, C.; Martín, Á. Reversible hydrogen sorption in the composite made of magnesium borohydride and silica aerogel. *Int. J. Hydrog. Energy* **2016**, *41*, 15245–15253. [CrossRef]
18. Kim, J.; Shim, J.; Cho, Y.W. On the reversibility of hydrogen storage in Ti- and Nb-catalyzed $Ca(BH_4)_2$. *J. Power Sources* **2008**, *181*, 140–143. [CrossRef]
19. Hino, S.; Fonneløp, J.E.; Corno, M.; Zavorotynska, O.; Damin, A.; Richter, B.; Baricco, M.; Jensen, T.R.; Sørby, M.H.; Hauback, B.C. Halide substitution in magnesium borohydride. *J. Phys. Chem. C* **2012**, *116*, 12482–12488. [CrossRef]
20. Ibikunle, A.A.; Goudy, A.J. Kinetics and modeling study of a $Mg(BH_4)_2$/$Ca(BH_4)_2$ destabilized system. *Int. J. Hydrog. Energy* **2012**, *37*, 12420–12424. [CrossRef]
21. Dematteis, E.M.; Vaunois, S.; Pistidda, C.; Dornheim, M.; Baricco, M. Reactive Hydride Composite of Mg_2NiH_4 with Borohydrides Eutectic Mixtures. *Crystals* **2018**, *8*, 90. [CrossRef]
22. Durojaiye, T.; Ibikunle, A.; Goudy, A.J. Hydrogen storage in destabilized borohydride materials. *Int. J. Hydrog. Energy* **2010**, *35*, 10329–10333. [CrossRef]
23. Dematteis, E.M.; Pistidda, C.; Dornheim, M.; Baricco, M. Exploring Ternary and Quaternary Mixtures in the $LiBH_4$-$NaBH_4$-KBH_4-$Mg(BH_4)_2$-$Ca(BH_4)_2$ System. *ChemPhysChem* **2019**, *20*, 1348–1359. [CrossRef] [PubMed]
24. Paskevicius, M.; Ley, M.B.; Sheppard, D.A.; Jensen, T.R.; Buckley, C.E. Eutectic melting in metal borohydrides. *Phys. Chem. Chem. Phys.* **2013**, *15*, 19774–19789. [CrossRef] [PubMed]
25. Dematteis, E.M.; Pinatel, E.R.; Corno, M.; Jensen, T.R.; Baricco, M.; Sturari, S.; Pistidda, C.; Baricco, M. Phase diagrams of the $LiBH_4$–$NaBH_4$–KBH_4 system. *Phys. Chem. Chem. Phys.* **2017**, *19*, 25071–25079. [CrossRef] [PubMed]
26. Jensen, S.R.H.; Jepsen, L.H.; Skibsted, J.; Jensen, T.R. Phase Diagram for the $NaBH_4$-KBH_4 System and the Stability of a Na(1−x)K(x)BH_4 Solid Solution. *J. Phys. Chem. C* **2015**, *119*, 27919–27929. [CrossRef]
27. Ley, M.B.; Roedern, E.; Jensen, T.R. Eutectic melting of $LiBH_4$–KBH_4. *Phys. Chem. Chem. Phys.* **2014**, *16*, 24194–24199. [CrossRef] [PubMed]
28. Dematteis, E.M.; Roedern, E.; Pinatel, E.R.; Corno, M.; Jensen, T.R.; Baricco, M. A thermodynamic investigation of the $LiBH_4$–$NaBH_4$ system. *RSC Adv.* **2016**, *6*, 60101–60108. [CrossRef]
29. Lutterotti, L.; Matthies, S.; Wenk, H.R. MAUD: A friendly Java program for material analysis using diffraction. *IUCr Newsl. CPD* **1999**, *21*, 14–15.
30. D'Anna, V.; Lawson Daku, L.M.; Hagemann, H. Vibrational spectra and structure of borohydrides. *J. Alloys Compd.* **2013**, *580*, S122–S124. [CrossRef]
31. D'Anna, V.; Spyratou, A.; Sharma, M.; Hagemann, H. FT-IR spectra of inorganic borohydrides. *Spectrochim. Acta Part A Mol. Biomol. Spectrosc.* **2014**, *128*, 902–906. [CrossRef]
32. Fichtner, M.; Chlopek, K.; Longhini, M.; Hagemann, H. Vibrational Spectra of $Ca(BH_4)_2$. *J. Phys. Chem. C* **2008**, *112*, 11575–11579. [CrossRef]
33. Borgschulte, A.; Gremaud, R.; Züttel, A.; Martelli, P.; Remhof, A.; Ramirez-Cuesta, A.J.; Refson, K.; Bardaji, E.G.; Lohstroh, W.; Fichtner, M.; et al. Experimental evidence of librational vibrations determining the stability of calcium borohydride. *Phys. Rev. B* **2011**, *83*, 024102. [CrossRef]
34. Hagemann, H.; D'Anna, V.; Rapin, J.P.; Černý, R.; Filinchuk, Y.; Kim, K.C.; Sholl, D.S.; Parker, S.F. New fundamental experimental studies on α-$Mg(BH_4)_2$ and other borohydrides. *J. Alloys Compd.* **2011**, *509*, 2010–2012. [CrossRef]

35. Filinchuk, Y.; Cerny, R.; Hagemann, H.; Černý, R. Insight into Mg $(BH_4)_2$ with synchrotron X-ray diffraction: structure revision, crystal chemistry, and anomalous thermal expansion. *Chem. Mater.* **2009**, *21*, 925–933. [CrossRef]
36. Černý, R.; Penin, N.; Hagemann, H.; Filinchuk, Y. The First Crystallographic and Spectroscopic Characterization of a 3 d -Metal Borohydride: $Mn(BH_4)_2$. *J. Phys. Chem. C* **2009**, *113*, 9003–9007. [CrossRef]
37. Dimitrievska, M.; White, J.L.; Zhou, W.; Stavila, V.; Klebanoff, L.E.; Udovic, T.J. Structure-dependent vibrational dynamics of $Mg(BH_4)_2$ polymorphs probed with neutron vibrational spectroscopy and first-principles calculations. *Phys. Chem. Chem. Phys.* **2016**, *18*, 25546–25552. [CrossRef]
38. Liu, A.; Xie, S.; Dabiran-Zohoory, S.; Song, Y. High-Pressure Structures and Transformations of Calcium Borohydride Probed by Combined Raman and Infrared Spectroscopies. *J. Phys. Chem. C* **2010**, *114*, 11635–11642. [CrossRef]
39. Shannon Database of Ionic Radii. Available online: http://abulafia.mt.ic.ac.uk/shannon/ptable.php (accessed on 20 May 2019).
40. Stadie, N.P.; Callini, E.; Richter, B.; Jensen, T.R.; Borgschulte, A.; Züttel, A. Supercritical N_2 processing as a route to the clean dehydrogenation of porous $Mg(BH_4)_2$. *J. Am. Chem. Soc.* **2014**, *136*, 8181–8184. [CrossRef]
41. Chong, M.; Karkamkar, A.; Autrey, T.; Orimo, S.; Jalisatgi, S.; Jensen, C.M. Reversible dehydrogenation of magnesium borohydride to magnesium triborane in the solid state under moderate conditions. *Chem. Commun.* **2011**, *47*, 1330–1332. [CrossRef]
42. Chong, M.; Matsuo, M.; Orimo, S.; Autrey, T.; Jensen, C.M. Selective Reversible Hydrogenation of $Mg(B_3H_8)_2/MgH_2$ to $Mg(BH_4)_2$: Pathway to Reversible Borane-Based Hydrogen Storage? *Inorg. Chem.* **2015**, *54*, 4120–4125. [CrossRef] [PubMed]
43. Riktor, M.D.; Sørby, M.H.; Chłopek, K.; Fichtner, M.; Buchter, F.; Züttel, A.; Hauback, B.C. In situ synchrotron diffraction studies of phase transitions and thermal decomposition of $Mg(BH_4)_2$ and $Ca(BH_4)_2$. *J. Mater. Chem.* **2007**, *17*, 4939. [CrossRef]
44. He, L.; Li, H.-W.; Tumanov, N.; Filinchuk, Y.; Akiba, E. Facile synthesis of anhydrous alkaline earth metal dodecaborates $MB_{12}H_{12}$ (M = Mg, Ca) from $M(BH_4)_2$. *Dalt. Trans.* **2015**, *44*, 15882–15887. [CrossRef] [PubMed]
45. Mao, J.; Guo, Z.; Poh, C.K.; Ranjbar, A.; Guo, Y.; Yu, X.; Liu, H. Study on the dehydrogenation kinetics and thermodynamics of $Ca(BH_4)_2$. *J. Alloys Compd.* **2010**, *500*, 200–205. [CrossRef]
46. Kim, Y.; Reed, D.; Lee, Y.-S.; Lee, J.Y.; Shim, J.; Book, D.; Cho, Y.W. Identification of the Dehydrogenated Product of $Ca(BH_4)_2$. *J. Phys. Chem. C* **2009**, *113*, 5865–5871. [CrossRef]
47. Kim, Y.; Hwang, S.; Lee, Y.S.; Suh, J.; Han, H.N.; Cho, Y.W. Hydrogen Back-Pressure Effects on the Dehydrogenation Reactions of $Ca(BH_4)_2$. *J. Phys. Chem. C* **2012**, *116*, 25715–25720. [CrossRef]
48. Minella, C.B.; Pistidda, C.; Garroni, S.; Nolis, P.; Baró, M.D.; Gutfleisch, O.; Klassen, T.; Bormann, R.; Dornheim, M. $Ca(BH_4)_2 + MgH_2$: Desorption Reaction and Role of Mg on Its Reversibility. *J. Phys. Chem. C* **2013**, *117*, 3846–3852. [CrossRef]
49. Muetterties, E.L.; Merrifield, R.E.; Miller, H.C.; Knoth, W.H.; Downing, J.R. Chemistry of Boranes. III. 1 The Infrared and Raman Spectra of $B_{12}H_{12}$ -and Related Anions. *J. Am. Chem. Soc.* **1962**, *84*, 2506–2508. [CrossRef]